



HAL
open science

The role of baroclinic activity in controlling Earth's albedo in the present and future climates

Or Hadas, George Datselis, Joaquin Blanco, Sandrine Bony, Rodrigo Caballero, Bjorn Stevens, Yohai Kaspi

► **To cite this version:**

Or Hadas, George Datselis, Joaquin Blanco, Sandrine Bony, Rodrigo Caballero, et al.. The role of baroclinic activity in controlling Earth's albedo in the present and future climates. Proceedings of the National Academy of Sciences of the United States of America, 2023, 120, 10.1073/pnas.2208778120 . insu-04196542

HAL Id: insu-04196542

<https://insu.hal.science/insu-04196542>

Submitted on 5 Sep 2023

HAL is a multi-disciplinary open access archive for the deposit and dissemination of scientific research documents, whether they are published or not. The documents may come from teaching and research institutions in France or abroad, or from public or private research centers.

L'archive ouverte pluridisciplinaire **HAL**, est destinée au dépôt et à la diffusion de documents scientifiques de niveau recherche, publiés ou non, émanant des établissements d'enseignement et de recherche français ou étrangers, des laboratoires publics ou privés.



Distributed under a Creative Commons Attribution - NonCommercial - NoDerivatives 4.0 International License



The role of baroclinic activity in controlling Earth's albedo in the present and future climates

Or Hadas^{a,1}, George Datsieris^b, Joaquin Blanco^c, Sandrine Bony^d, Rodrigo Caballero^c, Bjorn Stevens^b, and Yohai Kaspi^a

Edited by Timothy Palmer, University of Oxford, Oxford, United Kingdom; received May 22, 2022; accepted November 16, 2022

Clouds are one of the most influential components of Earth's climate system. Specifically, the midlatitude clouds play a vital role in shaping Earth's albedo. This study investigates the connection between baroclinic activity, which dominates the midlatitude climate, and cloud-albedo and how it relates to Earth's existing hemispheric albedo symmetry. We show that baroclinic activity and cloud-albedo are highly correlated. By using Lagrangian tracking of cyclones and anticyclones and analyzing their individual cloud properties at different vertical levels, we explain why their cloud-albedo increases monotonically with intensity. We find that while for anticyclones, the relation between strength and cloudiness is mostly linear, for cyclones, in which clouds are more prevalent, the relation saturates with strength. Using the cloud-albedo strength relationships and the climatology of baroclinic activity, we demonstrate that the observed hemispheric difference in cloud-albedo is well explained by the difference in the population of cyclones and anticyclones, which counter-balances the difference in clear-sky albedo. Finally, we discuss the robustness of the hemispheric albedo symmetry in the future climate. Seemingly, the symmetry should break, as the northern hemisphere's storm track response differs from that of the southern hemisphere due to Arctic amplification. However, we show that the saturation of the cloud response to storm intensity implies that the increase in the skewness of the southern hemisphere storm distribution toward strong storms will decrease future cloud-albedo in the southern hemisphere. This complex response explains how albedo symmetry might persist even with the predicted asymmetric hemispheric change in baroclinicity under climate change.

storm tracks | clouds | climate change

Earth's surface temperature is proximately determined by its atmospheric infrared transmissivity, the planetary albedo, and the net solar insolation. Of these, the albedo is thought to be determined by small-scale processes that regulate surface properties and the distribution of particulate matter, especially clouds, in the atmosphere (1). This raises the question as to whether the coupling between albedo and global climate is mediated by small-scale processes, the distribution of which is perhaps selected by the climate, or whether the large-scale circulation (for instance, as measured by pole-to-equator temperature gradients) alone might inform estimates of the distribution of clouds and hence planetary albedo, and thereby more directly link albedo to climate. Such links would greatly aid efforts to develop conceptual models of the climate system. In this study, we explore the basis for such links, focusing on extratropical clouds.

The extratropics, and in particular the midlatitudes, play a vital role in shaping Earth's albedo due to their significant contribution to cloud-albedo (Fig. 1A). An intriguing phenomenon that involves midlatitude clouds is the hemispheric symmetry in reflected shortwave radiation: Satellite-based estimates of Earth's top-of-the-atmosphere radiation budget show that the Northern- and Southern-Hemisphere (NH and SH, respectively) reflect almost the same amount of short-wave radiation (relative difference smaller than 0.1%), while the relative hemispheric difference in clear-sky reflectance is more than 10% (2–4). This symmetry is part of a larger class of hemispheric symmetry problems, such as the hemispheric symmetry in total precipitation (5), which are a striking property of the Earth's climate, given the hemispheric difference in continental configuration. The large discrepancy between the clear-sky albedo and planetary albedo is mainly due to clouds (1, 6–8), as in Earth's current climate, clouds form such that the total outgoing shortwave radiation is hemispherically symmetric. Analysis of the climatology of cloud-albedo (Fig. 1A, 9, 10) reveals that the biggest contributors are the midlatitudes. Furthermore, the hemispheric difference in the zonal mean cloud-albedo is also dominated by the midlatitudes, where the SH extratropical cloud-albedo is significantly higher (Fig. 1C).

Significance

We find a strong connection between the magnitude of midlatitude storminess and cloud-albedo, thereby linking the large-scale circulation to the planetary albedo. We use this linkage to propose a mechanism for the observed similarity in reflected sunlight between the two hemispheres: The presence of more ocean causes the southern-hemisphere to absorb more sunlight; however, it also makes it stormier, increasing cloud-albedo and balancing the difference in reflected sunlight. Due to the changes in storminess predicted by CMIP6 models, this link also implies less cloud-albedo with warming and a possible break of hemispheric albedo symmetry. For this symmetry to persist, the distribution of southern-hemisphere storms should shift to fewer but stronger storms, as predicted by climate-change models.

Author contributions: O.H., S.B., R.C., B.S., and Y.K. designed research; O.H. performed the calculations and analyzed the data; Y.K. supervised the research; O.H., G.D., J.B., S.B., R.C., B.S., and Y.K. contributed to the discussions; and O.H. and Y.K. wrote the paper.

The authors declare no competing interest.

This article is a PNAS Direct Submission.

Copyright © 2023 the Author(s). Published by PNAS. This open access article is distributed under Creative Commons Attribution-NonCommercial-NoDerivatives License 4.0 (CC BY-NC-ND).

¹To whom correspondence may be addressed. E-mail: or.hadas@weizmann.ac.il.

This article contains supporting information online at <http://www.pnas.org/lookup/suppl/doi:10.1073/pnas.2208778120/-/DCSupplemental>.

Published January 27, 2023.

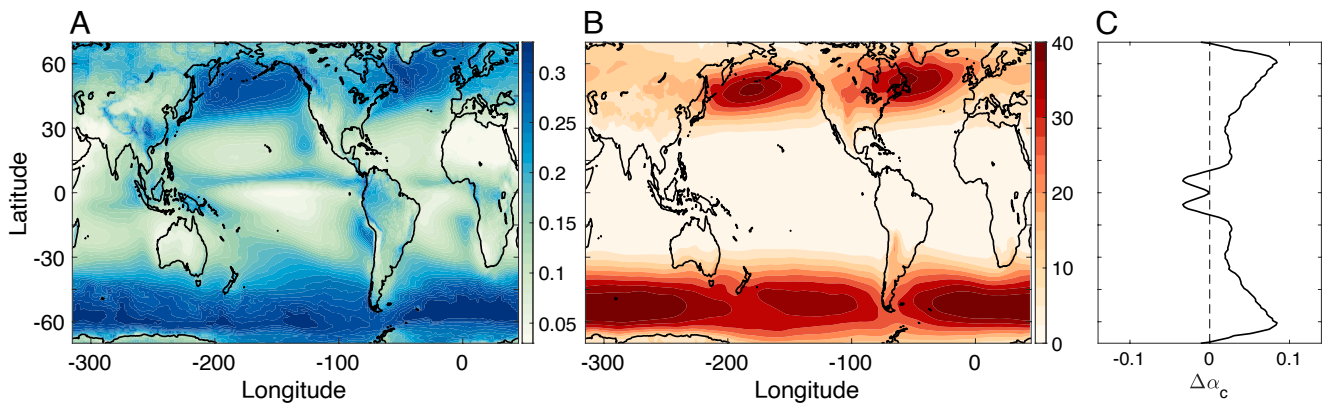


Fig. 1. (A) Climatology of cloud-albedo. (B) Climatology of synoptic scale activity, defined as $E = \overline{\text{SLP}'^2}$, where the bar stands for the time mean and the prime is defined as the high-pass of zonal wavenumbers above five of the sea-level pressure (SLP). (C) The hemispheric difference (SH minus NH) in zonal mean cloud-albedo as a function of latitude. The cloud-albedo is calculated from CERES short-wave flux data, following the method presented in (1). Data for A and C is the daily mean data from CERES and data for B is taken from ERA5, as described in *Materials and Methods*.

This study proposes that baroclinic activity, which dominates midlatitude dynamics, mediates between the general circulation, cloudiness, and planetary albedo. Previous work, which focused primarily on cyclones, showed that different parts of the cyclones and anticyclones are selective for different types of clouds, (11–13). The warm eastern part of cyclones is characterized by layered mid- and high-level clouds, which at the cyclone front turn into a fully developed cloud, filling most of the atmospheric column, accompanied by significant precipitation. These clouds are associated with the warm conveyor belt (13). The upstream region of the cyclone front is characterized by low clouds, which are associated with the cold conveyor belt. Cyclone strength strongly affects the cloud regimes, and it has been shown that the high clouds and the shortwave radiation forcing associated with the cyclones positively correlate with their strength (14, 15).

To link the cloud-albedo to large-scale circulation and the hemispheric albedo symmetry, the response of the cloud field to the cyclone and anticyclone intensity is investigated and then used to connect the hemispheric difference in storm track activity and cloud-albedo, which reveals the role of baroclinic activity in the symmetry. Previous studies of NH and SH storm tracks (16–18) revealed several key differences: First, in the annual mean, the SH storm track is stronger, both with respect to the NH zonal mean and the Pacific and Atlantic storm tracks. This is evident when considering Eulerian properties such as Eddy Kinetic Energy (EKE) or Lagrangian properties such as cyclone track density and average intensity (19). Second, the NH storm track undergoes a stronger seasonal cycle, with the winter storm track being almost three times more intense than the summer one, due to a significant decrease in summer baroclinicity. Conversely, the SH storm track seasonality is mostly a meridional shift, which was found to enhance cloudiness in high latitudes during mid-winter (20). Third, the NH storm track is much less zonally symmetric, with most of the storm activity occurring over the Pacific and Atlantic Oceans, while, over the continents, storm activity is suppressed (21).

We use a combination of CERES satellite data (22, 23) and ERA5 reanalysis data (24) to reveal the effect of baroclinic activity on the midlatitude cloud-albedo. The CERES short-wave fluxes are used to calculate the cloud-albedo. The ERA5 sea-level pressure is used to characterize synoptic weather system (SWS) activity from an Eulerian perspective. A feature tracking

algorithm is used to identify individual SWS (25), which allows us to characterize the storm track also from a Lagrangian perspective. We also use ERA5 cloud cover data at different heights, which cannot be reliably done using satellite images because highly developed clouds, which are often present in the warm sector (and fronts) of cyclones, block observations of low- and medium-level clouds (*Material and Methods* for an in-depth discussion of data sources). Feature tracking is advantageous in this context as it allows us to study how the presence and properties of a SWS affect the cloud field around it. Using the insights from the analysis, we deduce how the hemispheric difference in baroclinic activity relates to the hemispheric albedo symmetry. We then show how the hemispheric albedo symmetry might persist in the future climate, given the predicted change in baroclinic activity due to global warming.

The Effect of Baroclinic Activity on Clouds

Eulerian Characteristics. The strong relation between baroclinic activity, here assessed using sea level pressure (SLP, taken from ERA5 reanalysis) variance (26, 27) and midlatitude cloud-albedo (calculated using CERES data) can be seen clearly in the climatology (Fig. 1 A and B), as the peaks of cloud-albedo are located at regions with strong baroclinic activity. Indeed, the spatial correlation between the climatology of cloud-albedo and baroclinic activity over the midlatitudes (latitudes 30° to 60° in both hemispheres) is 0.86 with a negligible P -value. The close correlation between baroclinic activity and cloud-albedo motivates us to address how the correlation emerges from a single-storm perspective.

Cloud Composites. To show how the high correlation between baroclinic activity and cloud-albedo emerges from the effect of the single SWS on the cloud fields in its vicinity, we analyze composites of cloud-albedo from CERES and cloud cover at different levels from ERA5 (Fig. 2, *Materials and Methods* for an in-depth discussion of tracking and composites) for cyclones and anticyclones in three strength categories: the lowest 40%, the 40 to 70%, and the highest 30% (hereafter weak, medium, and strong SWSs, respectively).

Focusing first on the medium-strength cyclones (Fig. 2 E–H), a high cloud-albedo region poleward and eastward to the cyclone center is detected. This feature is associated with cloud

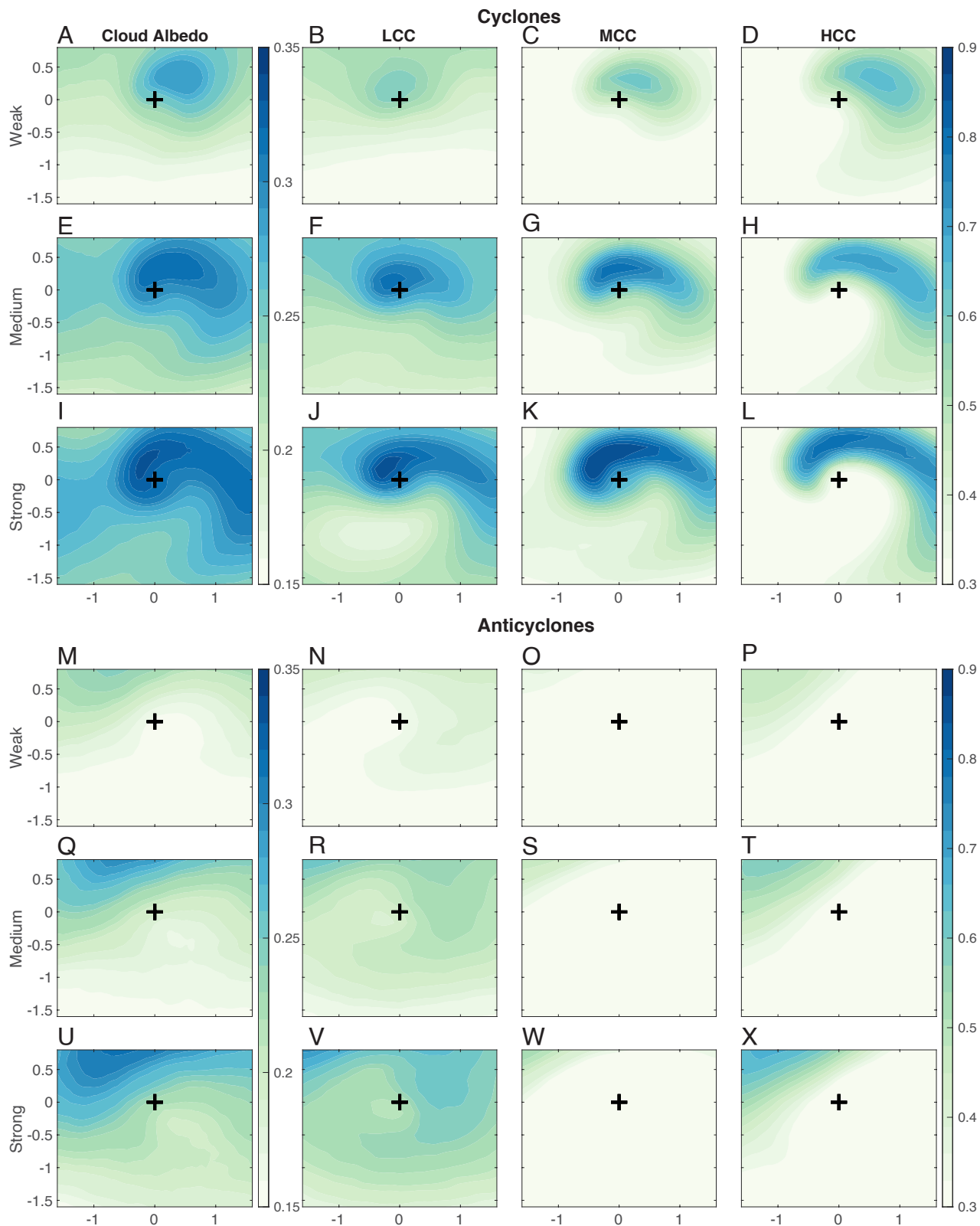


Fig. 2. Composite of the cloud-albedo (*A*, *E*, and *I*), low cloud cover (LCC, *B*, *F*, and *J*), middle cloud cover (MCC, *C*, *G*, and *K*), and high cloud cover (HCC, *D*, *H*, and *L*), averaged over cyclones of the lowest 40% (*A–D*), between the 40 and 70% (*E–H*) and for the highest 30% in intensity (*I–L*). The abscissa and ordinate are the zonal and meridional distances (10^3 km) from the cyclone center (black crosses). The SH cyclones were flipped in the meridional direction, so positive values in the ordinate will mean poleward for all cyclones. (*M–X*) Same as (*A–L*) but for anticyclones. Cloud-albedo is calculated based on CERES data and cloud data, and SWS tracks are based on ERA5 data.

cover at all heights. This high albedo anomaly was previously reported for the cloud shortwave radiative effect (14, 28) and is associated with the warm sector and the updraft of the cyclone (29, 30). Southwest of the cyclone center, an anomalously low cloud-albedo region appears, associated with the cold sector and the sinking air on the west-side of the cyclone. Besides these two patterns, the region surrounding the cyclone is primarily cloudy with low cloud cover (LCC), which has a moderate contribution to cloud-albedo. Composites of anticyclones (Fig. 2 *M–X*) show an anomalously clear region in mid-level cloud cover (MCC) and high-level cloud cover (HCC) and a peak in LCC to the east of the center, due to subsidence in the cold sector of the anticyclone (30, 31). The surrounding MCC and HCC peaks are a result of nearby cyclones in the composite.

Comparing the cloud-albedo of SWSs composites with different strengths reveals that stronger SWSs have substantially higher cloud-albedo (Fig. 2 *A, E, and I*). The intensification can be divided into two modes of response: the first mode increases the peak of the cloud-albedo in the eastern, warm sector and spreads the cloud stripe equatorward. This increase is due to stronger cyclones typically having more intense warm conveyor belts and updrafts (30). The increase appears at all levels (Fig. 2 *B, F, and J* for LCC, Fig. 2 *C, G, and K* for MCC, and Fig. 2 *D, H, and L* for HCC), showing that the entire atmospheric column is becoming cloudier. The second mode is an increase in LCC at the outer edges of the cyclones composite. This mode is associated with stronger cold advection and more vigorous mixing of the boundary layer by the stronger surface winds in strong cyclones (32, 33).

A more elaborate investigation of the composite mean cloud-albedo response to the SWS's intensity reveals that the cloud-albedo-strength relation increases monotonically (Fig. 3 *A* and *B* for cyclones and anticyclones, respectively). To ensure that the observed relation is not due to distribution biases (e.g., because the SWSs in the SH are both stronger and cloudier), we plot the relation for the NH and the SH (blue and red curves, respectively). For a given surface pressure anomaly, there are small differences in SH versus NH composites, with the SH SWSs being slightly cloudier. However, these differences are small compared to the changes in cloud-albedo as a function of the surface pressure anomaly (about 25% vs. 4%). These trends are also robust when we take a smaller composite box that includes only the core of the SWSs (*SI Appendix, Fig. S1*).

An intriguing result is that the cloud-albedo-strength relation saturates for cyclones. To understand this trend, we decompose the cloud-albedo response to the response of total cloud cover and optical thickness (TCC and τ respectively, *SI Appendix, Fig. S2 A–D*), which relate to cloud-albedo through Eq. 4 in (9). Both properties generally increase with cyclones' strength and saturate for strong cyclones. This saturation for TCC is because TCC is a bound quantity, and the entire box approaches overcast (about 90% cast, *SI Appendix, Fig. S2A*). The saturation in τ is mostly due to the warm sector being close to saturation, while the cold sector is selective for shallow clouds, which do not span the entire atmospheric column (Fig. 2 *I–L*), and is therefore characterized by a low optical thickness. Another trend that appears in the cloud properties of cyclones and anticyclones is that the SH TCC is larger than the NH TCC (*SI Appendix, Fig. S2 A and B*), which is balanced by a larger NH optical thickness (*SI Appendix, Fig. S2 C and D*). The ERA5 TCC as a function of SWS strength (*SI Appendix, Fig. S2 E and F*) also demonstrates both monotonic increases with strength and saturation for cyclones, which means these trends are robust across satellite and reanalysis data. The main differences between reanalysis and satellite data are that

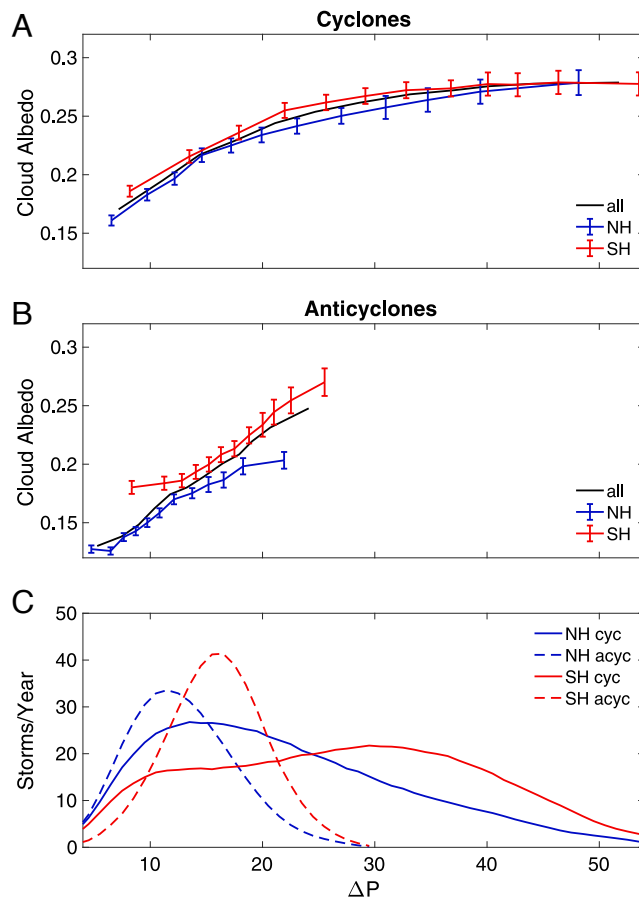


Fig. 3. Composite mean cloud-albedo as a function of cyclone (*A*) and anticyclone (*B*) intensity (hPa surface anomaly). Each point represents the mean of the 10, 20, 30, 40, 50, 60, 70, 80, 85, 90, and 95% for all SWSs (black solid) and for the NH and SH (blue and red, respectively). (*C*) The yearly number of cyclones (solid) and anticyclones (dashed) for a given intensity (hPa surface anomaly) for the NH (blue) and SH (red). Cloud-albedo is calculated based on CERES data, and cyclone and anticyclone tracks are based on ERA5 data. The composite average area is as defined in *Materials and Methods*. Error bars are defined as one SD from the mean value. A similar analysis using CERES and ERA5 cloud properties is presented in *SI Appendix, Fig. S1*.

the cyclone TCC curves (*SI Appendix, Fig. S2 A and E*) saturate on a value lower by about 10% and that the TCC hemispheric difference for a given cyclone strength is much smaller.

Implications for Climate

Hemispheric Cloud-Albedo Asymmetry. Using the findings above, we now show how the hemispheric asymmetry in cloud-albedo can be largely understood from the differences in baroclinic activity. A track density map of the weak, medium, and strong cyclones and anticyclones (*SI Appendix, Fig. S3*) shows that weak cyclones (*SI Appendix, Fig. S3A*) distribute evenly between land and ocean and are more common in the NH (350 cyclones in the NH relative to 240 in the SH). On the other hand, the medium and strong cyclones (*SI Appendix, Fig. S3 B and C*) are more common in the SH (360 cyclones in the NH and 520 in the SH) and are rare over NH continents. Repeating the analysis for anticyclones (*SI Appendix, Fig. S3 D–F*) shows that, similar to cyclones, most of the weak anticyclones are in the NH and many appear over land, while the medium and strong anticyclones are more abundant in the SH and over the oceans.

When considering the overall yearly amount of SWSs tracked for the NH and SH (Fig. 3C), we find that the SH SWSs are stronger and more abundant. On average, in the NH, there are annually about 710 cyclones with an average intensity of 20 hPa and 580 anticyclones with an average intensity of 12 hPa, while over the SH, there are 760 cyclones with an average intensity of 25 hPa and 650 anticyclones with an average intensity of 15 hPa (the annual amount was calculated by integrating over the distribution, and mean intensity was defined as the distribution average).

Because stronger SWSs are shown to be cloudier, we can associate the hemispheric difference in cloud-albedo with the difference in baroclinic activity: because the SWSs in the SH are stronger, they create more clouds. To quantify this, we analyze to which extent the difference in baroclinic activity explains the difference in cloud-albedo. Assuming that

$$\begin{aligned} \alpha_{\text{cyc}} &\sim \sum_i \sigma(s_i) \cdot N_i, \\ \alpha_{\text{acyc}} &\sim \sum_i \lambda(s_i) \cdot N_i, \\ \alpha &= \alpha_{\text{cyc}} + \alpha_{\text{acyc}}, \end{aligned} \quad [1]$$

where α_{cyc} and α_{acyc} are the cyclone's and anticyclone's contribution to cloud-albedo, respectively, σ and λ are the functions connecting intensity and cloud-albedo for cyclones and anticyclones, respectively, s_i is the strength of each bin (taken here to be the SWS's maximum pressure anomaly), and N_i is the number of SWSs per year in each strength bin. In order to increase the accuracy of our estimates, we interpolate the observed connections between strength and cloud-albedo by fitting a curve to the observed relation (black line in Fig. 3A and B). The functions used for cyclones and anticyclones are

$$\begin{aligned} \sigma(s) &= \frac{a}{1 + \exp[-b \cdot (s + c)]}, \\ \lambda(s) &= a + b \cdot s, \end{aligned} \quad [2]$$

where σ is the sigmoid function, which was chosen because of its saturating properties and λ is the linear function. The parameters a , b , and c for σ and a and b for λ are found by fitting to cloud-albedo strength relations for cyclones and anticyclones, as was found for CERES data (black line in Fig. 3A and B, respectively) and are given in the *SI Appendix, Table S1*. Using the ERA5 baroclinic SWS statistics (Fig. 3C), the calculated difference is 15.7%, where cyclones contribute 8.4% and anticyclones contribute 7.3%, while the climatological difference in cloud-albedo is 14.1% for CERES data. These results show that the difference in cloud-albedo between the NH and SH can be predicted by the difference in baroclinic activity. Thus, baroclinic activity increases the SH albedo by roughly how much the land asymmetry increases the NH albedo.

These findings give a possible mechanism for the compensation between clear-sky and cloud-albedo: the hemisphere with more ocean (and thus less clear-sky albedo) generates more baroclinic activity, which creates more clouds and thus results in higher cloud-albedo. This counterbalances the higher clear-sky albedo in the hemisphere with more continents. Further analysis of the connection between the hemispheric difference in clear-sky albedo and baroclinic activity might reveal why the overall planetary albedo is exactly the same in the two hemispheres. A possible theoretical framework for such an explanation might be the conservation of global isentropic potential vorticity, known

as the Impermeability Theorem (34), which was shown recently to play a significant role in shaping tropical weather (35).

Albedo Symmetry in Future Climate. Clouds are one of the most significant uncertainties in the climate response to the anthropogenic increase in greenhouse gases (36, 37). The strong connection between baroclinic activity and cloud-albedo links cloudiness to macroscopic circulation features, which may then influence how albedo changes with warming. The baroclinic activity response to climate change, assessed using the CMIP6 models (*Materials and Methods*), is different in the two hemispheres, where the NH activity is expected to weaken due to arctic amplification (38–40) while SH is expected to slightly strengthen (Fig. 4A). The strong relation between baroclinic activity and cloudiness implies a large decrease in the NH midlatitude cloud-albedo, while the SH cloudiness is projected to intensify slightly. As no significant hemispheric asymmetry in the response of surface albedo to climate change is predicted (8), this allegedly implies that the hemispheric albedo symmetry should break.

However, the Lagrangian analysis shows how the albedo symmetry can still be maintained. Considering the cyclones' intensity distribution in current and future climate (Fig. 4B, (41)), a substantial decrease in the frequency of weak and medium cyclones (9.1% fewer relative to the overall number of cyclones) is expected both in the NH and SH. Yet, the SH baroclinic activity intensifies due to a small increase in the frequency of strong cyclones (2.0% more relative to the overall number of cyclones). While the contribution of the strong cyclones to SLP variance is very large (as their degree of contribution corresponds to their depth to the second power), the saturating nature of the cloud-albedo strength curve of cyclones (Fig. 3A) means their contribution to cloud-albedo is not as large, which explains how cloud-albedo might decline over the SH to maintain the hemispheric albedo symmetry. To quantify this statement, we use Eq. 1 and assume that

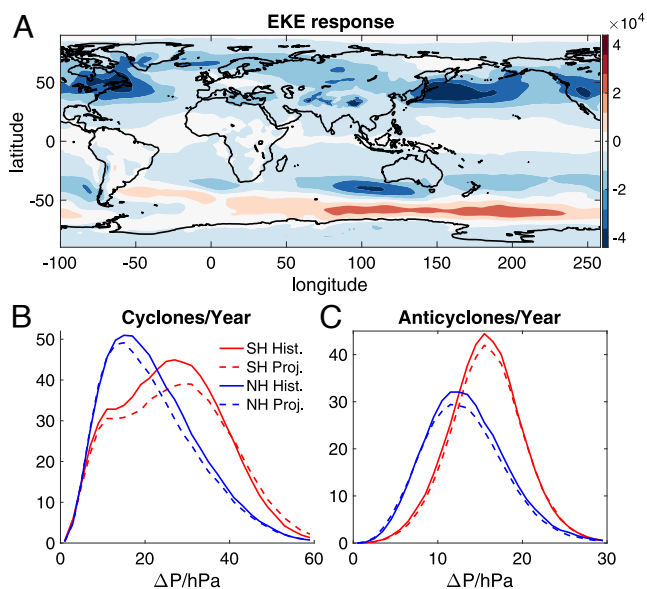


Fig. 4. (A) Response of baroclinic activity (hPa^2) to climate change. Baroclinic activity is defined as in Fig. 1B. The response is defined as the change in climatological between the projected and historical simulations (*Materials and Methods*). (B and C) The probability distribution function of cyclone and anticyclone intensity for the NH and SH (blue and red, respectively) for the historical and projected runs (solid and dash lines, respectively).

$$\text{EKE} \sim \sum_i s_i^2 \cdot N_i,$$

where s_i is the strength of each bin and N_i is the number of cyclones per year in each strength bin. Using the CMIP6 models' average values (Fig. 4B), we find no significant change in EKE in the SH, even though the cloud-albedo decreases by 6.8%. Over the NH, we find a decrease of 9.4% in EKE and 7.6% in cloud-albedo. This shows that a decrease in cloud-albedo can result from both a decrease in the overall baroclinicity (as found over the NH) and an increase in the skewness of the intensity distribution (without a significant change in the overall baroclinic activity, as found over the SH). The anticyclone response (Fig. 4C) is similar between hemispheres: a reduction in the number of anticyclones and a projected decrease in their contribution to cloud-albedo.

Summary and Discussion

The effect of Earth's atmospheric circulation on clouds and the cloud feedback on the circulation through their effect on the radiation budget is a significant source of complexity in climate research and an active field of study (42–44). Therefore, studying large-scale climate phenomena that reflect fundamental properties of the cloud–climate interaction can aid in understanding Earth's climate and its susceptibility to change. In this study, we investigate the role of baroclinic activity in shaping Earth's albedo through clouds. More specifically, we uncover the role of baroclinic activity in the hemispheric difference in cloud-albedo: the difference in the layout of the continents between the two hemispheres, leads to stronger baroclinic activity in the SH such that the clouds resulting from it compensate for the asymmetry in clear-sky albedo. Our results can be summarized as follows:

- There is a strong spatial correlation between cloud-albedo and baroclinic activity (Fig. 1).
- Composites of cyclones and anticyclones show that strong synoptic weather systems (SWSs) have higher cloud-albedo (Fig. 2). This indicates that the magnitudes of both phases of baroclinic waves monotonically increase cloud-albedo.
- This monotonic increase in cloud-albedo is due to the equatorward extending and thickening of cloud bands in the warm sectors and the increase in low clouds in the cold sectors of cyclones, and more low clouds around the center of anticyclones (Fig. 2).
- A more detailed view of the connection between SWS strength and cloudiness shows that while the connection in the case of anticyclones is strictly linear, the cloud-albedo curve saturates for strong cyclones (Fig. 3).
- The track distribution reveals that the weaker, less cloudy SWSs are primarily present in the NH, while the stronger, cloudier SWSs mostly appear over the SH and the NH oceans (SI Appendix, Fig. S2).
- The hemispheric difference in cloud-albedo can be quantitatively estimated using the cloud-albedo strength relation for cyclones and anticyclones (Fig. 3A and B) and the climatology of baroclinic activity (Fig. 3C). The calculated difference is 15.7%, while the CERES difference is 14.1%.
- Our findings suggest a possible mechanism for the similar reflected short-wave radiation between the two hemispheres: the greater ocean area in the SH, and therefore lower surface albedo, causes it to have stronger baroclinic activity, which, in

turn, creates more clouds, which balance the overall planetary albedo.

- Due to the strong connection between baroclinic activity and cloudiness, the response of baroclinic activity to climate change will affect the cloud distribution.
- In future climate, the expected decrease in EKE over the NH (Fig. 4A) implies a significant decrease in the NH midlatitude cloud-albedo.
- Over the SH, the projected change in the distribution of cyclone intensity (Fig. 4B and C) suggests that the SH cloud-albedo will to decrease, although the overall EKE will increase.
- This complex response shows how hemispheric albedo symmetry might persist in the future climate, despite the asymmetric response of EKE.

Materials and Methods

Climate Data. To study the current climate, we use a combination of reanalysis and satellite data. We use 3-h data from the European Centre for Medium-Range Weather Forecasts (ECMWF) ERA-5 data set (24) to assess the synoptic weather system (SWS) activity and track. ERA-5 estimates the atmospheric variables at a horizontal resolution of 31 km and 137 vertical levels. Sea level pressure (SLP) is used to quantify the midlatitude baroclinic activity and to identify and track cyclones and anticyclones. We also use 3-h data of low-, mid-, and high-cloud cover (LCC, MCC, and HCC, respectively) to assess the vertical distribution of clouds. Three-hourly total cloud cover (TCC) data were also used to compare to satellite data. To assess short-wave radiation fluxes and cloud properties, we use the Clouds and the Earth's Radiant Energy System (CERES) SYN1 deg-day version 4a product (22, 23). CERES's clear- and all-sky short wave fluxes are used to calculate cloud-albedo, using the method described in ref. 9. TCC and optical thickness (τ) are used to decompose the cloud-albedo into the contribution of the two different cloud properties (9, 45, 46). Cloud data were downloaded on a 3-h resolution, and cloud-albedo was calculated on a daily resolution and then resampled to a 3-h resolution, based on the data Fourier spectrum. We use data between the years 2001 and 2019.

To assess predicted changes in baroclinic activity due to climate change, we use 6-h SLP data from the Coupled Model Intercomparison Project phase 6 (CMIP6, list of models is provided in SI Appendix, Table S2). We use the years 1980 to 2010 of the historical data and the end of the century (2070 to 2100) of the Shared Socioeconomic Pathway 5-8.5 (SSP5-8.5) scenario for projected data.

Storm Tracking and Composites. Cyclones and anticyclones are identified and tracked using an objective feature point tracking technique (25) applied on SLP. The algorithm gives the longitude, latitude ($^{\circ}$), and magnitude of the anomaly (hPa) in each time step through its lifetime. We filter the data and smooth it to T63 resolution, to reduce noise, and removed background flow (defined as wave numbers 0 to 4) to isolate the synoptic and mesoscale features. Only anomalies deeper than 8 hPa that appear for more than 48 h and pass latitude 30° are used in the analysis. We also require a traveling distance of more than 1,000 km for cyclones. SI Appendix, Fig. S3 shows the distribution of tracked cyclones and anticyclones at maximum intensity, showing that the tracked storms generally fit well the position of the storm tracks. Some bias can be observed around high topography, mostly for weak SWSs. Filtering out tracks around high topography does not change significantly any of the results.

To construct composites, we place a box with margins at a distance of $\pm 1,600$ km in the zonal direction and -1670 to 830 km in the meridional direction from the center of the SLP anomaly, and then pick the maximum intensity time-step. The meridional direction of SH SWSs was flipped to match the NH SWSs. Overall, roughly 52,000 cyclones and 43,000 anticyclones are used for the composites. The composite we achieve using ERA5 data resembles the results of previous studies, which use cloud fields from various sources, e.g., refs. 15, 47 and 48.

Data, Materials, and Software Availability. All study data are included in the article and/or *SI Appendix*.

ACKNOWLEDGMENTS. We thank Shira Raveh-Rubin, Hisashi Nakamura, and the reviewers for their helpful comments. This research has been supported by the Israeli Science Foundation (Grant 996/20), European Union's Horizon 2020 research and innovation programme under Grant Agreement 820829

1. G. Datsis, B. Stevens, Earths albedo and its symmetry. *AGU Adv.* **2**, e2021AV000440 (2021).
2. G. L. Stephens *et al.*, The albedo of Earth. *Rev. Geophys.* **53**, 141–163 (2015).
3. T. H. Vonder Haar, V. E. Suomi, Measurements of the earth's radiation budget from satellites during a five-year period. Part i. Extended time and space means. *J. Atmos. Sci.* **28**, 305–314 (1971).
4. B. Stevens, S. E. Schwartz, Observing and modeling earth's energy flows. *Surv. Geophys.* **33**, 779–816 (2012).
5. A. Voigt, B. Stevens, J. Bader, T. Mauritsen, The observed hemispheric symmetry in reflected shortwave irradiance. *J. Climate* **26**, 468–477 (2013).
6. P. J. Webster, *Dynamics of the Tropical Atmosphere and Oceans* (John Wiley and Sons, 2020).
7. V. Ramanathan, The role of earth radiation budget studies in climate and general circulation research. *J. Geophys. Res. (Atmos.)* **92**, 4075–4095 (1987).
8. V. Ramanathan *et al.*, Cloud-radiative forcing and climate: Results from the earth radiation budget experiment. *Science* **243**, 57–63 (1989).
9. A. Donohoe, D. S. Battisti, Atmospheric and surface contributions to planetary albedo. *J. Climate* **24**, 4402–4418 (2011).
10. F. A. M. Bender, A. Engström, R. Wood, R. J. Charlson, Evaluation of hemispheric asymmetries in marine cloud radiative properties. *J. Clim.* **30**, 4131–4147 (2017).
11. K. A. Browning, *Organization of Clouds and Precipitation in Extratropical Cyclones in Extratropical Cyclones* (Springer, 1990), pp. 129–153.
12. N. C. Lau, M. W. Crane, Comparing satellite and surface observations of cloud patterns in synoptic-scale circulation systems. *Mon. Weath. Rev.* **125**, 3172–3189 (1997).
13. G. Tselioudis, K. M. Grise, "Midlatitude cloud systems in Clouds and climate: Climate science's greatest challenge" in A. P. Siebesma, S. Bony, C. Jakob, B. Stevens, Eds. (Cambridge University Press, 2020).
14. G. Tselioudis, W. B. Rossow, Climate feedback implied by observed radiation and precipitation changes with midlatitude storm strength and frequency. *Geophys. Res. Lett.* **33** (2006).
15. P. R. Field, R. Wood, Precipitation and cloud structure in midlatitude cyclones. *J. Climate* **20**, 233–254 (2007).
16. B. J. Hoskins, K. I. Hodges, A new perspective on southern hemisphere storm tracks. *J. Climate* **18**, 4108–4129 (2005).
17. T. A. Shaw *et al.*, Storm track processes and the opposing influences of climate change. *Nat. Geosci.* **9**, 656–664 (2016).
18. B. Hoskins, K. Hodges, The annual cycle of northern hemisphere storm tracks. Part i: Seasons. *J. Climate* **32**, 1743–1760 (2019).
19. T. Tamarin-Brodsky, Y. Kaspi, Enhanced poleward propagation of storms under climate change. *Nat. Geosci.* **10**, 908–913 (2017).
20. K. L. Verlinden, D. W. Thompson, G. L. Stephens, The three-dimensional distribution of clouds over the southern hemisphere high latitudes. *J. Climate* **24**, 5799–5811 (2011).
21. Y. Kaspi, T. Schneider, The role of stationary eddies in shaping midlatitude storm tracks. *J. Atmos. Sci.* **70**, 2596–2613 (2013).
22. S. Kato *et al.*, Surface irradiances of edition 4.0 clouds and the earth's radiant energy system (CERES) energy balanced and filled (EBAF) data product. *J. Clim.* **31**, 4501–4527 (2018).
23. N. G. Loeb *et al.*, Clouds and the earth's radiant energy system (CERES) energy balanced and filled (EBAF) top-of-atmosphere (TOA) edition-4.0 data product. *J. Clim.* **31**, 895–918 (2018).
24. H. Hersbach *et al.*, The ERA5 global reanalysis. *Q. J. R. Meteorol. Soc.* **146**, 1999–2049 (2020).
25. K. Hodges, Feature tracking on the unit sphere. *Mon. Weath. Rev.* **123**, 3458–3465 (1995).
26. H. Nakamura, Midwinter suppression of baroclinic wave activity in the Pacific. *J. Atmos. Sci.* **49**, 1629–1642 (1992).
27. E. K. M. Chang, S. Lee, K. L. Swanson, Storm track dynamics. *J. Climate* **15**, 2163–2183 (2002).
28. A. Bodas-Salcedo *et al.*, Large contribution of supercooled liquid clouds to the solar radiation budget of the southern ocean. *J. Climate* **29**, 4213–4228 (2016).
29. J. F. Booth, L. Polvani, P. A. O'Gorman, S. Wang, Effective stability in a moist baroclinic wave. *Atmos. Sci. Lett.* **16**, 56–62 (2015).
30. T. Tamarin-Brodsky, O. Hadas, The asymmetry of vertical velocity in current and future climate. *Geophys. Res. Lett.* **46**, 374–382 (2019).
31. K. M. Grise, B. Medeiros, J. J. Benedict, J. G. Olson, Investigating the influence of cloud radiative effects on the extratropical storm tracks. *Geophys. Res. Lett.* **46**, 7700–7707 (2019).
32. J. R. Norris, S. F. Jacobellis, North pacific cloud feedbacks inferred from synoptic-scale dynamic and thermodynamic relationships. *J. Clim.* **18**, 4862–4878 (2005).
33. L. Nuijens, B. Stevens, The influence of wind speed on shallow marine cumulus convection. *J. Atmos. Sci.* **69**, 168–184 (2012).
34. P. H. Haynes, M. E. McIntyre, On the evolution of vorticity and potential vorticity in the presence of diabatic heating and frictional or other forces. *J. Atmos. Sci.* **44**, 828–841 (1987).
35. S. Ortega, P. J. Webster, V. Toma, H. R. Chang, The effect of potential vorticity fluxes on the circulation of the tropical upper troposphere. *Q. J. R. Meteorol. Soc.* **144**, 848–860 (2018).
36. A. Voigt *et al.*, Clouds, radiation, and atmospheric circulation in the present-day climate and under climate change. *Wiley Interdiscip. Rev.: Clim. Change* **12**, e694 (2021).
37. P. Forster *et al.*, "The earth's energy budget, climate feedbacks, and climate sensitivity" in *Climate Change 2021: The Physical Science Basis. Contribution of Working Group I to the Sixth Assessment Report of the Intergovernmental Panel on Climate Change* (Cambridge University Press, 2021).
38. J. Yuval, Y. Kaspi, Eddy activity response to global warming-like temperature changes. *J. Climate* **33**, 1381–1404 (2020).
39. R. Chemke, L. M. Polvani, Linking midlatitudes eddy heat flux trends and polar amplification. *npj Clim. Atmos. Sci.* **3**, 1–8 (2020).
40. D. Kim, S. M. Kang, T. M. Merlis, Y. Shin, Atmospheric circulation sensitivity to changes in the vertical structure of polar warming. *Geophys. Res. Lett.* **48**, e2021GL094726 (2021).
41. E. K. M. Chang, Projected significant increase in the number of extreme extratropical cyclones in the southern hemisphere. *J. Climate* **30**, 4915–4935 (2017).
42. P. Ceppi, D. L. Hartmann, Connections between clouds, radiation, and midlatitude dynamics: A review. *Curr. Clim. Change Rep.* **1**, 94–102 (2015).
43. Y. Li, D. W. Thompson, S. Bony, T. M. Merlis, Thermodynamic control on the poleward shift of the extratropical jet in climate change simulations: The role of rising high clouds and their radiative effects. *J. Climate* **32**, 917–934 (2019).
44. P. Ceppi, P. Nowack, Observational evidence that cloud feedback amplifies global warming. *Proc. Natl. Acad. Sci. U.S.A.* **118** (2021).
45. A. A. Lacis, J. Hansen, A parameterization for the absorption of solar radiation in the earth's atmosphere. *J. Atmos. Sci.* **31**, 118–133 (1974).
46. R. Caballero, *Physics of the Atmosphere* (IOP Publishing Bristol, 2014), vol. 150.
47. A. Bodas-Salcedo, K. Williams, P. Field, A. Lock, The surface downwelling solar radiation surplus over the Southern Ocean in the Met Office model: The role of midlatitude cyclone clouds. *J. Climate* **25**, 7467–7486 (2012).
48. C. M. Naud, J. F. Booth, A. D. Del Genio, Evaluation of ERA-interim and MERRA cloudiness in the southern ocean. *J. Climate* **27**, 2109–2124 (2014).

(CONSTRAIN project), the Yotam project, the Weizmann Institute Sustainability and Energy Research Initiative, and the Azrieli fellowship.

Author affiliations: ^aDepartment of Earth and Planetary Sciences, Weizmann Institute of Science, 76100 Rehovot, Israel; ^bMax-Planck-Institut für Meteorologie, D-20146 Hamburg, Germany; ^cDepartment of Meteorology, Stockholm University, 10691 Stockholm, Sweden; and ^dSorbonne Université, Laboratoire de Météorologie Dynamique (LMD)/Institut Pierre Simon Laplace (IPSL), Centre National de la Recherche Scientifique (CNRS), Univ Paris 06, 75252 Paris, France